Composites Part B 190 (2020) 107947

Contents lists available at ScienceDirect

Composites Part B

journal homepage: www.elsevier.com/locate/compositesb

Microstructure, mechanical properties, and in-vitro biocompatibility of nano- NiTi reinforced Mg–3Zn-0.5Ag alloy: Prepared by mechanical alloying for implant applications

Mahmood Razzaghi , Masoud Kasiri-Asgarani *, Hamid Reza Bakhsheshi-Rad **, Hamid Ghayour

Advanced Materials Research Center, Department of Materials Engineering, Najafabad Branch, Islamic Azad University, Najafabad, Iran

ARTICLE INFO

Keywords:
Mg-based nanocomposites
Mechanical alloying
Mechanical properties
Nitinol
Biocompatibility

ABSTRACT

A sort of biodegradable magnesium-based nanocomposites improved by nano-sized NiTi particles has been offered in the current research with the evaluations for implant application. The samples were provided through mechanical alloying followed by sintering; the assessments consisted of microstructure, mechanical properties, and in-vitro biocompatibility. The impacts of integrating 15, 30, and 45 wt% of NiTi nano-particles on the characteristics of Mg–3Zn-0.5Ag magnesium alloy matrix have been investigated. The addition of 15 wt% of NiTi led to a decline in the grain size by 10.5%, an increase in the compressive strength by 56%, and a rise in the elongation by 7.6% as compared to the matrix; whereas further reinforcement addition reduced the elongation and compressive strength. The addition of 15 wt% NiTi causes a minor increase in corrosion rate, but incorporating 30 and 45 wt% of NiTi content result a major increase in corrosion rate. The improved compressive mechanical properties may be ascribed to Hall-Petch impact, the load transfer from matrix to NiTi particles, Orowan strengthening mechanism, and locking of dislocations owing to the occurrence of hard NiTi reinforcement particles. In-vitro biocompatibility tests such as MTT and DAPI assay revealed that the nanocomposites are appropriate for medical uses. It may be stated that the nanocomposite comprising 15 wt% of NiTi can be used appropriately as an orthopedic implant biomaterial.

1. Introduction

Metallic biomaterials are primarily produced by cobalt-chrome alloys, stainless steel, and titanium. They are poor in biocompatibility, produce toxic metallic ions in the body of the human, have high weight and Young's modulus that trigger stress shielding and also require secondary surgery for removing the implant. Owing to such restrictions, the idyllic implant ought to be bio-compatible and bio-degradable with the same mechanical properties as natural bone [1,2]. Magnesium and its alloys are light metals with 1.74–2 g/cm3 density that are similar to the density of the natural bone. Mg-based implants are osteoconductive, biocompatible, and biodegradable with elasticity modulus like the natural bone. The magnesium ion is among the vital parts of the body that are primarily deposited in bones [3,4]. Owing to their capability to biodegrade in situ with no need for extra surgery to eradicate biodegradable implants, there is significant study interest in them [5,6].

Magnesium should be improved for implant applications despite high specific strength. To enhance the magnesium characteristics, alloying and forming magnesium-matrix biocomposites have been carried out [7]. One method to enhance magnesium strength is using suitable alloying elements, such as aluminum, calcium, zinc, cerium, silver, and thorium [8]. Mg–Zn alloys draw interest in medical applications as all the alloying elements occur naturally in the body with natural metabolism and release capabilities. The mechanical properties and corrosion resistance can be improved by up to 5 wt% of zinc in Mg–Zn binary over forming secondary phase, solid solution, and grain refinement [9]. The Zn impact on microstructure, mechanical properties, as well as magnesium corrosion behavior was investigated by Koç et al. However, inferior antibacterial capabilities are reported for Magnesium based composites, which result in infected implants, and as a result, post-operative issues. Silver antimicrobials were of concern as an alternative strategy to reduce bacterial adhesion and inhibiting the growth of biofilms. Silver's comprehensive antimicrobial action is recognized against both gram-positive and gram-negative bacteria,

* Corresponding author.
** Corresponding author.
E-mail addresses: m.kasiri.a@gmail.com (M. Kasiri-Asgarani), rezabakhsheshi@gmail.com (H.R. Bakhsheshi-Rad).

https://doi.org/10.1016/j.compositesb.2020.107947
Received 24 September 2019; Received in revised form 17 February 2020; Accepted 2 March 2020
Available online 4 March 2020

Fig. 1. A schematic illustration of the fabrication process and evaluations of the nanocomposites (Graphical abstract).

Table 1
Designation, nominal compositions, densities and porosity of the matrix and nanocomposites.

Sample Name (Code)		Composition (wt.%)				Theoretical Density (g/cc)	Experimental Density (g/cc)	Porosity (%)
		Mg	Zn	Ag	NiTi			
Matrix	(M)	96.50	3.00	0.50	0.00	1.782	1.711	3.98
Matrix-15NiTi	(C15)	82.03	2.55	0.43	15.00	1.998	1.913	4.25
Matrix-30NiTi	(C30)	67.55	2.10	0.35	30.00	2.275	2.167	4.75
Matrix-45NiTi	(C45)	53.08	1.65	0.28	45.00	2.642	2.511	4.99

Table 2
Parameters of the mechanical alloying process adopted for milling the powders.

Parameter	Value
Rotation speed	300 rpm
Ball-Powder weight ratio	15:1
Vial and ball material	Steel
Mass of powder	30 g
Milling time	25 h
Capacity of the vial	250 ml
Diameter of the balls	20 mm

protozoa, fungi, and particular viruses as antibiotic-resistant strains [10,11]. A minute Ag addition may also enhance the mechanical properties of Mg alloys [12–14]. Zhang et al. showed that the microstructure was refined, and the second phase volume was raised following the addition of Ag to the Mg–Nd–Zn–Zr alloys [15]. Ag and Ca incorporation into the Mg–2.4Zn alloy may also enhance the mechanical properties and corrosion resistance [16].

Composite strengthening mechanism is one of the feasible paths to improve the mechanical properties of magnesium alloys [17]. Various types of reinforcements can be used for strengthening the matrix including particles, short fibers or whiskers, continuous fibers and plates [18–24]. The applications of particle reinforced composite materials reinforcements have been increasing in various areas of technology due to their good performance and properties [25–31]. Even though ceramic reinforcements like B_4C, SiC, Y_2O_3, TiC, Al_2O_3, and TiB_2 may increase the magnesium-based matrix strength, the fabricated composite formability is decreased owing to the formation of brittle phases in areas of the matrix-reinforcement interface. The formability problem may be solved via metallic reinforcements, such as Ni, Cu, and Ti [32]. NiTi alloy as a metallic reinforcement has decent mechanical properties and biocompatibility, and it is a proper choice for medical use [4,33–35]. Magnesium with 5, 10, and 15 vol% of micron-sized NiTi were reinforced by Esen. Based on the results, mechanical properties of magnesium may be improved by NiTi over grain refinement and incorporation in a composite. The composite encompassing 5 vol% (16.4 wt%) NiTi has the best results, and the mechanical properties reduced for the composites encompassing 10 and 15 vol% NiTi [36]. Using sintering fabrication technique, Wakeel et al. strengthened magnesium with 2 wt % of nano-sized NiTi. The outcomes revealed that the microhardness and compression strength have been raised by 30% as compared to the magnesium matrix [37].

To fabricate the magnesium-based composites, a possible method is to apply powder metallurgy paths (e.g., mechanical alloying, MA). To generate different non-equilibrium phases or alloys, such as supersaturated solid solutions, amorphous phases, nanostructured materials, and nanocomposites in powder form mechanical alloying is a solid-state reaction [38,39]. The mechanical characteristics of Mg-based biocomposites may be enhanced via mechanical alloying through the grain size modification as opposed to the as-cast Mg samples with larger grains, as well as uniformly dispersed reinforcement particles [40,41].

The current research, thus, aims primarily to study the

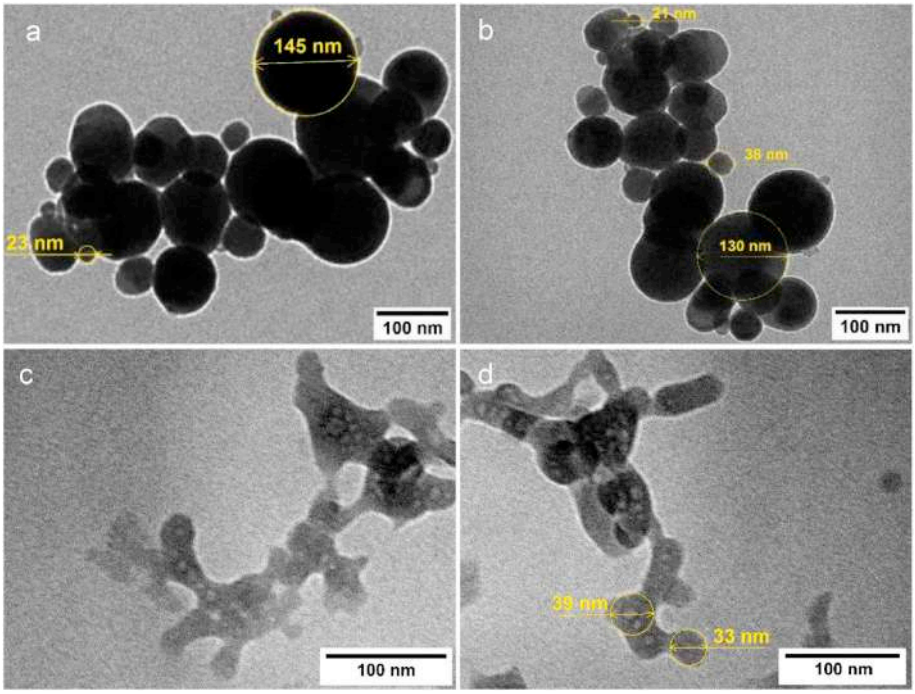

Fig. 2. TEM images (a, b) NiTi powder, (c, d) matrix milled powder.

microstructure, as well as mechanical and biological characteristics of Mg–3Zn–0.5Ag alloy, NiTi reinforced nanocomposite to define the NiTi impact on the characteristics.

2. Materials and methods

2.1. Sample preparation

Fig. 1 shows the schematic illustration of the fabrication procedure to provide the nanocomposites. The procedure begins by mixing pure magnesium powder (99.8% purity, 50 μm mean particle size), Ag powder (99.9% purity, 6.5 μm average particle size), Zn powder (98.8% purity, 7.5 μm mean particle size) bought from Sigma-Aldrich, USA as well as nano-sized NiTi powder (20–150 nm particle size). Table 1 demonstrates the composition and designation of the research nanocomposites. The procedure was accompanied by mechanical alloying, wherein Mg–3Zn-0.5Ag-xNiTi (x = 0, 15, 30, 45 wt%) composite powders have been indicated as M, C15, C30, and C45, respectively. For 25 h at room temperature, they were milled in an argon controlled atmosphere planetary ball mill. The charge was loaded into a steel vial with a purified argon (<3 ppm oxygen) atmosphere. To mill, stainless steel balls with the diameter 20 mm were utilize and the balls quantity of the vial was computed based on the ball to powder weight ratio of 15:1. Table 2 illustrates the factors of mechanical alloying approved to mill the nanocomposites [42,43].

By the pressure of 880 MPa for the compression test samples (φ6 × 9 mm) and 400 MPa for other test samples (Ø10 × 10 mm), the milled powders have been compressed. In the next step, the green compressed samples were sintered in two steps; 2 h at 200 °C and 2 h at 530 °C with 5 °C/min continuous heating rate in an argon controlled atmosphere,. The porosity of nanocomposites was computed on the basis of the equation: $Total\ porosity = (1 - \frac{Bulk\ density}{\rho_{composite}}) \times 100$. The nanocomposites theoretical density was computed on the basis of Mg, Zn, Ag, and NiTi percentage using the equation:

$\rho_{composite} = f_{Mg}\cdot\rho_{Mg} + f_{Zn}\cdot\rho_{zn} + f_{Ag}\cdot\rho_{Ag} + f_{NiTi}\cdot\rho_{NiTi}$. For bulk density measurement, the sample mass was alienated by its volume; whereas the mass was calculated via an accurate scale, and the volume was calculated via the sample dimensions. The density of the measured bulk was certified through the equation: $Bulk\ density = \frac{W_d}{W_w - W_s}$ [44]; the overall porosity entailing interconnected pore network was calculated, where W_d and W_s indicate the sample weight in dry- and water-soaked circumstances, respectively; and ρ is the nanocomposite theoretical density.

2.2. Structural characterization

A scanning electron microscopy (SEM; Quanta 200) and an optical microscope were applied to observe the balk and the post-compression fractured samples microstructurally. To investigate the NiTi and milled matrix powder, transmission electron microscopy (TEM; Phillips 208 m) was used. An X-ray diffractometer (Siemens D5000) was applied to disclose the phase components through Cu-Kα radiation (45 kV, 40 mA) with the angles of diffraction (2θ) range between 30 and 80° with a scanning rate of 4°/min. To end with, The Williamson–Hall method was applied to define the crystallite size according to the equation: $\frac{\beta}{2}\cot\theta = \frac{0.45\lambda}{Sin\ \theta D} + \varepsilon$. In the equation, λ specifies X-ray wavelength, β indicates diffraction peak width at the mid-height, and D is the mean crystallite size (nm). The formula ε and θ, show microstrain and the Bragg diffraction angle, respectively [45].

To find the wettability of the surface of matrix and nanocomposites, the surface water contact angles were analyzed using the sessile drop method with a video contact angle instrument (Dataphysics OCA 15) in air at room temperature with the drop size of 10 mL. Average value of the contact angle of each type of material was calculated by the results of three samples.

2.3. Mechanical properties

The cylindrical sintered nanocomposites with 6 mm diameter and 9 mm height were hard-pressed by the SANTAM (STM-50) universal testing device at a crosshead speed 0.1 mm/min and a load cell 10 kN at room temperature to assess the compressive strength. Vickers hardness tester (LECO M-400) with 300 g force measured microhardness values of the samples.

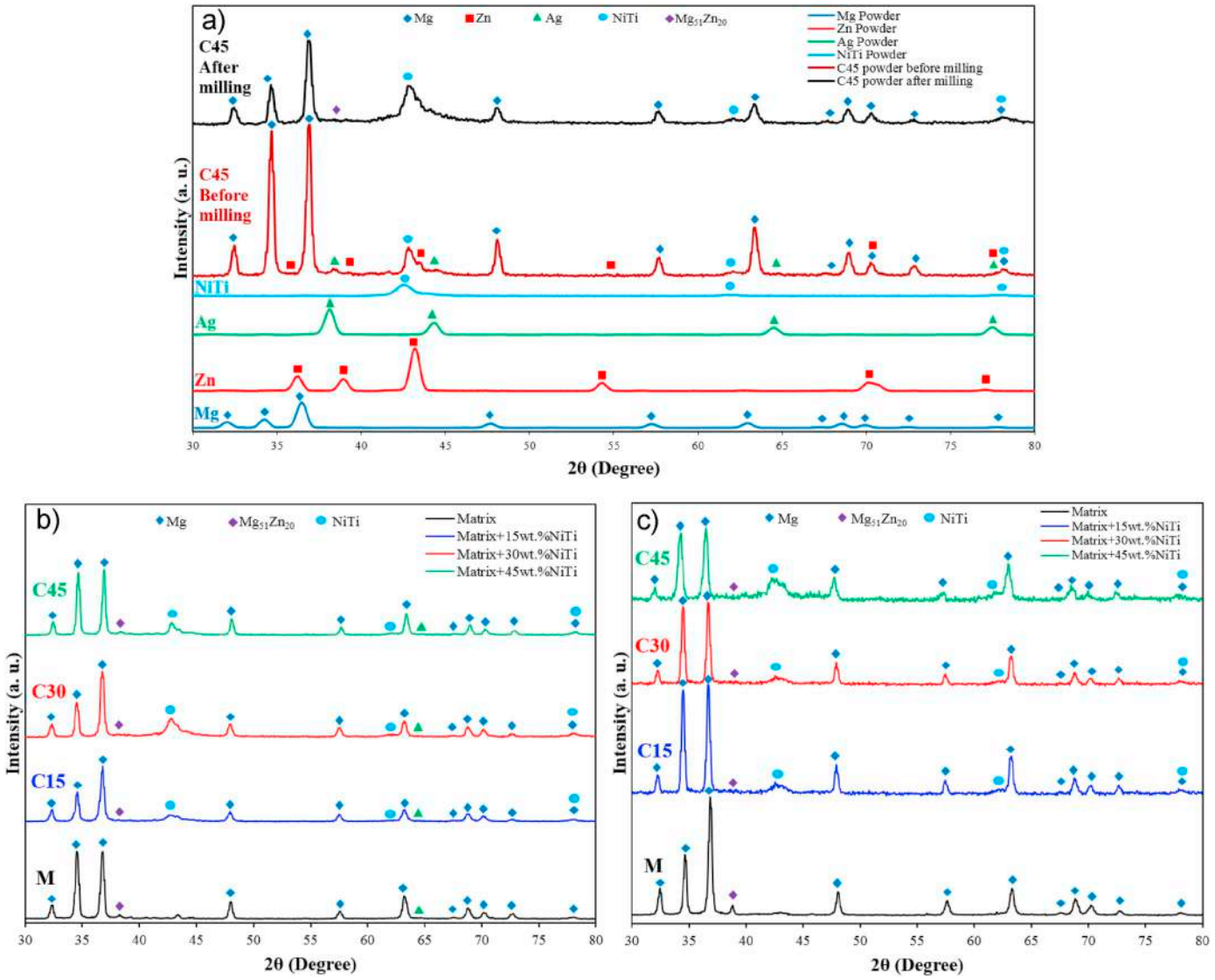

Fig. 3. XRD patterns of the matrix and nanocomposites a) XRD patterns of powder ingredients, C45 blended powder and C45 milled powder, b)Matrix and nanocomposites before sintering, and. c) Matrix and nanocomposites after sintering.

Table 3
Crystallite sizes of the matrix and nanocomposites before and after sintering.

Sample	Crystallite size (nm)	
	Before sintering	After sintering
Matrix	34.7	35.9
Matrix-15NiTi	28.9	32.8
Matrix-30NiTi	25.7	27.0
Matrix-45NiTi	24.3	26.1

2.4. In-vitro biocompatibility

The nanocomposite in vitro cytotoxicity encompassing NiTi was defined via indirect 3-(4,5-dimethylthiazol -2-yl)-2,5-diphenyltetrazolium-bromide (MTT, Sigma, Saint Louis, USA) assay on the basis of the extraction technique. The nanocomposites (5 mg) were added to the culture medium and incubated at 37 °C for 1 and 2 days. Then, 104 cells/ml were refined on the 96-well plates for 24 h; the cell medium was refreshed with 1 and 2-day extracts. After additional 24 h, the medium was removed, and 100 μL of the MTT agents (0.5 mg/mL in PBS) was inoculated into each well and was preserved for 4 h in the incubator. To dissolve the formazan crystals, 100 μl of DMSO was implanted into the well after 4 h. As a final point, the absorbance was read at 545 nm via an ELISA Reader (Stat Fax-2100, Miami, USA) and standardized via free nanocomposites culture medium as a control group. To study the MG63 cell proliferation on the nanocomposites encompassing NiTi under fluorescence microscopy, nuclear staining with DAPI (4′, 6-diamidino-2-phenylindole, blue fluorescence in live cells) was carried out.

2.5. Corrosion behavior

The nanocomposite samples with a surface area 0.8 cm^2 were provided and saturated in a three-electrode cell encompassing Kokubo SBF solution at 37 °C with a pH value of 7.4 according to Ref. [46] to perform the electrochemical measurements with PARSTAT 2273 potentiostat/galvanostat (Princeton Applied Research). The working electrode, in the cell, was applied with a platinum wire as the counter electrode, as well as a saturated calomel electrode (SCE) as the reference electrode. The readings of potentiodynamic polarization were from −250 to 1300 mV vs. open circuit potential (OCP) at a scan rate of 1 mV/s. Based on ASTM G1-03 [47], for the immersion test, the samples were immersed in 200 ml of Kokubo SBF solution (pH 7.4). Over the immersion test, the variation in the pH value of the SBF solution was recorded after each 24

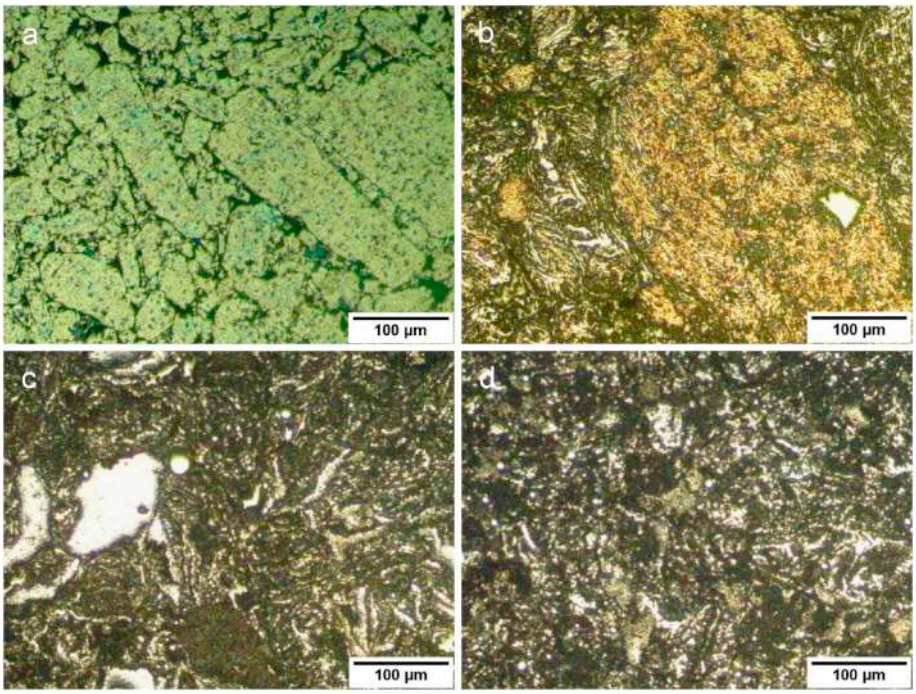

Fig. 4. Optical micrographs of the alloys (a) Matrix (b) Matrix-15NiTi, (c) Matrix-30NiTi, (d) Matrix-45NiTi.

h interval.

2.6. Statistical analysis

To disclose a meaningful difference between data, the results of the test were reported as mean ± standard error (SE), examined through Sigmaplot software with p-value <0.05 (*), p-value <0.01 (**), and p-value <0.001 (***).

3. Results and discussion

3.1. Density and porosity

The porosity and density of different samples in the research are presented in Table 1. The experimental and theoretical densities have been raised by increasing the NiTi as compared to the matrix that was expectable owing to a meaningful difference between the density of matrix (1.78 g/cc) and NiTi (6.45 g/cc). The maximum theoretical density of C45 sample is 2.64 g/cc that is approximately 48% higher than that of the matrix. The range of the porosity is around 4–5%. Under the same compaction pressure, nano-composites with higher NiTi content have higher porosity. It can be due to the possible debonding between the reinforcement and the matrix alloy. Moreover, the porosity can be controlled by compaction pressure adjustment. Additionally, the nanocomposite with higher pore quantities and sizes has higher biocompatibility but lower mechanical properties.

3.2. Microstructure characterization

The TEM micrographs of NiTi powder with the particle size range of 20–150 nm is presented in Fig. 2a–b. The particles, as seen, have spherical morphology. The TEM images of the milled powder are shown in Fig. 2c–d. The TEM images are related to the Mg–3Zn-0.5Ag matrix (M). As the morphology of the milled powders is similar, one of them is selected for presentation. The particle estimated dimension sizes 33 and 39 nm. The milled powder morphology is spherical, and the mechanical alloying process has caused cold welding between the milled powder particles and chain morphology of the milled powder.

The XRD patterns of the ingredients, mixed powder before milling, mechanically alloyed powders and the nano-composites after sintering process are illustrated in Fig. 3. The XRD patterns of the mechanically alloyed nano-composites revealed that the final products had no impurity. Before and after mechanical alloying, the C45 powder XRD patterns indicate a lower intensity of the major peaks in the milled powder. It may be because of the reduction of the particle size of the mechanically alloyed powder as compared with the powder before milling. After sintering, the peak intensity has fairly increased. This may be associated with increasing the grain size of the nanocomposites following heat treatment.

Crystallite size of the nanocomposites and matrix was computed according to the XRD results, as well as Williamson-Hall plot. The computed crystallite sizes are demonstrated in Table 3. The crystallite sizes of the milled matrix and nanocomposites, as can be observed, have been reduced by rising the content of NiTi. An increase in dislocations and a decrease in the crystallite size may arise by increasing the content of NiTi [48] as a result of interactions between hard NiTi nano-particles and dislocations. The crystallite size computed from 24.3 to 34.7 that validate the approximate measurement of the particle sizes in the TEM image. As can be seen, the crystallite size of the sintered matrix and nanocomposites has increased compared with the composites before the sintering process. With increasing the content of NiTi nanoparticles, the grain size decreases. Grain size consists of the agglomerations of the crystallite size. So, increasing the crystallinity of the material leads to the increase of the crystallite size and hence the increase of the grain size. Therefore, increasing the grain size means increasing the crystallite size [49].

The optical micrographs of the nanocomposites are shown in Fig. 4. A minimum clustering and sensible uniform distribution of NiTi reinforcement particles are observed for the nanocomposites. The comparison of the nanocomposite micrograph (Fig. 4b–d) with matrix optical one (Fig. 4a) revealed that the grain size declined by the occurrence of nano-sized NiTi particles.

The SEM micrographs of matrix and the nanocomposites with various NiTi content are illustrated in Fig. 5. The yellow arrows show the

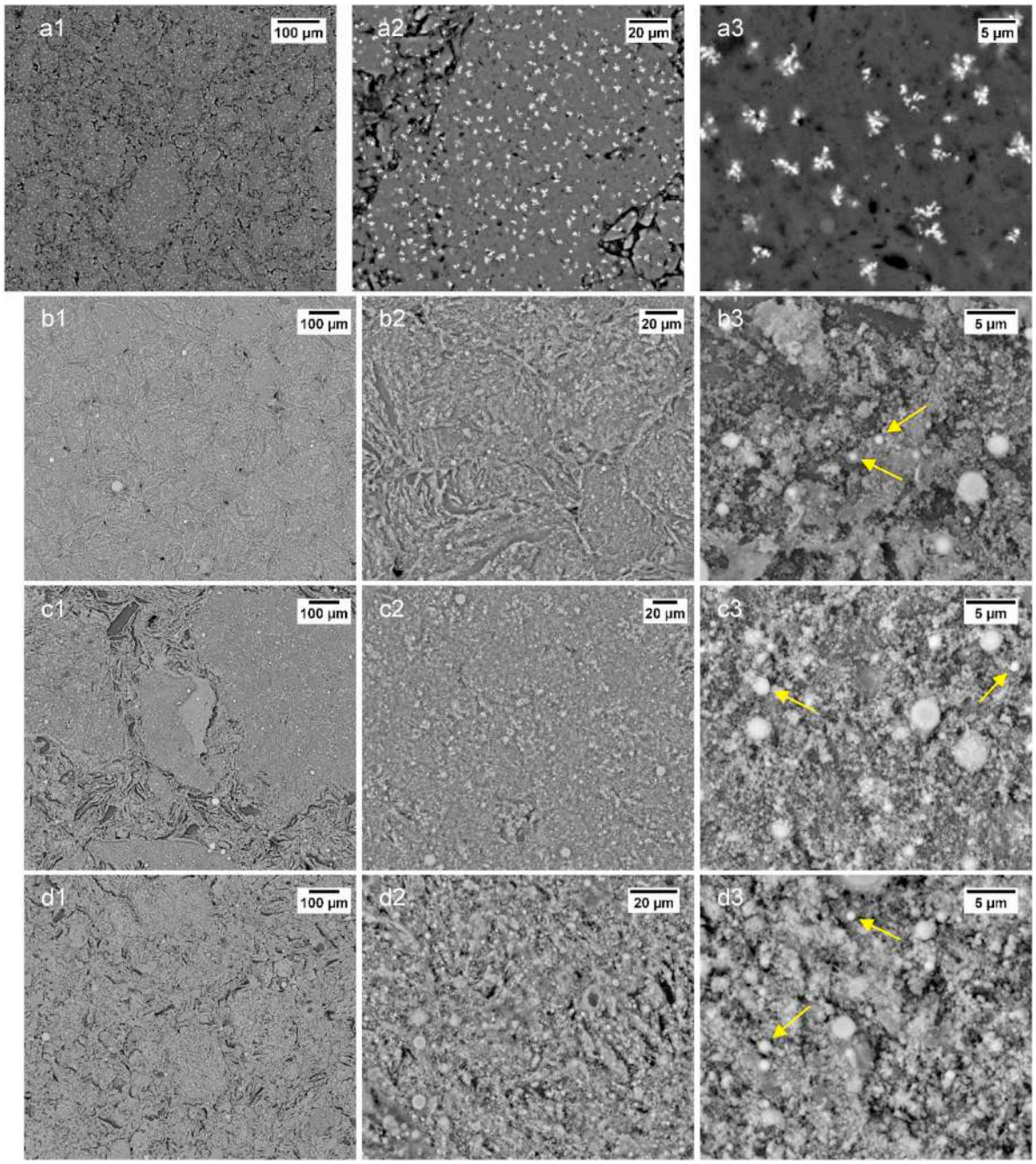

Fig. 5. SEM micrographs of (a1, a2, a3) Matrix, (b1, b2, b3) Matrix-15NiTi, (c1, c2, c3) Matrix-30NiTi and (d1, d2, d3) Matrix-45NiTi.

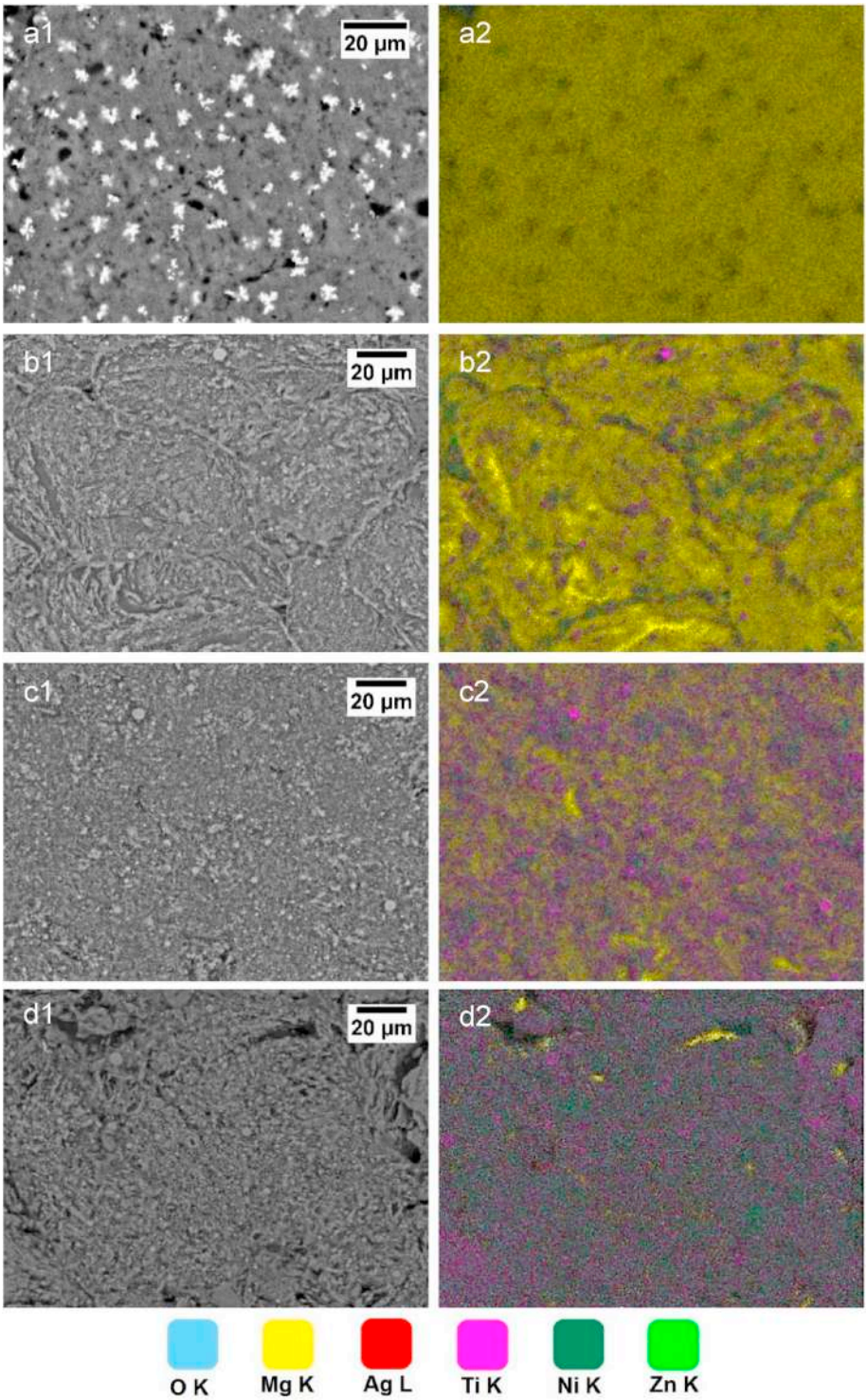

Fig. 6. SEM-EDS elemental mapping of Mg, Zn, Ag, Ni, Ti and O for (a1, a2) Matrix, (b1, b2) Matrix-15NiTi, (c1, c2) Matrix-30NiTi and (d1, d2) Matrix-45NiTi.

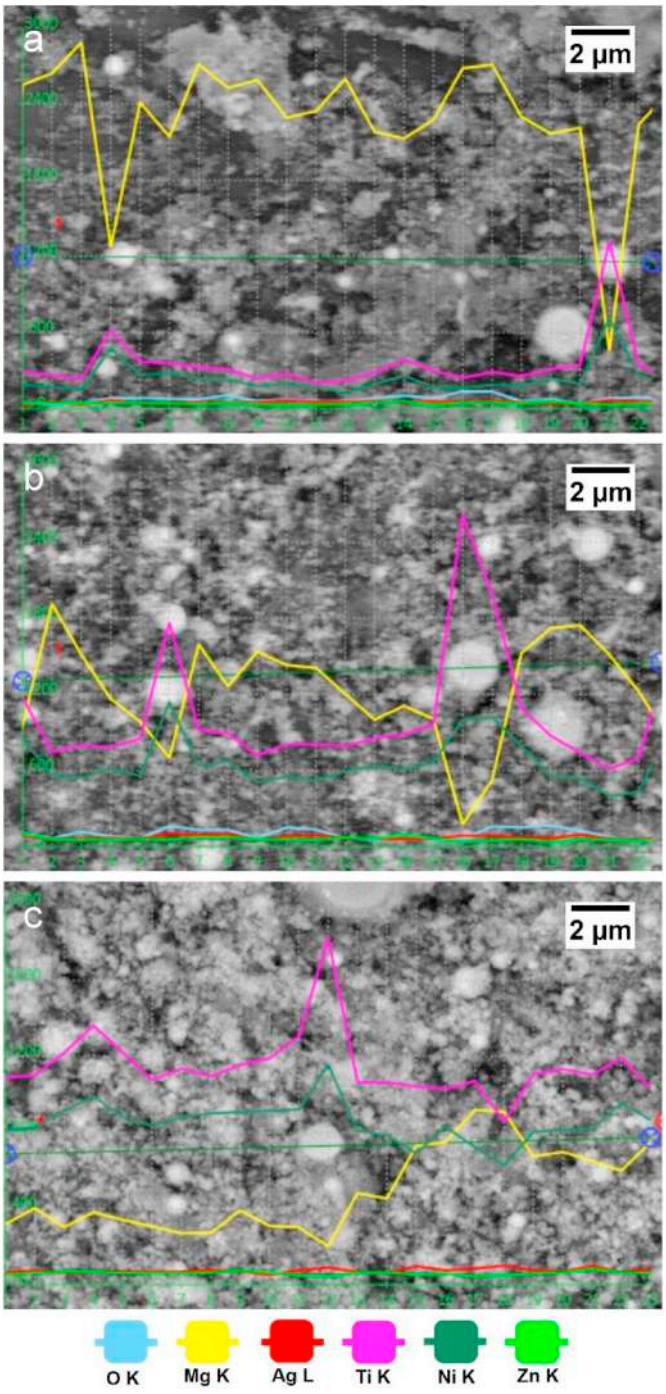

Fig. 7. SEM image and EDS line scan of Mg, Zn, Ag, Ni, Ti and O for (a1, a2) Matrix-15NiTi, (b1, b2) Matrix-30NiTi and (c1, c2) Matrix-45NiTi.

morphology of the NiTi particles. The nano NiTi particles' uniform distribution in the matrix are observed in a closer and more detailed sight. The reinforcement particles' uniform distribution may be ascribed to the mechanical alloying process nature, an idyllic combination of the powder ingredients throughout that.

The SEM-EDS elemental mapping of Ag, Mg, Zn, Ti, Ni, and O for the nanocomposites and matrix are demonstrated in Fig. 6. Dark green and pink colors show the presence of Ni and Ti elements as a result of NiTi nanoparticles existence. A rational uniform spread of NiTi particles is observed on the images of nanocomposite SEM-EDS in all nanocomposites. The dark green and pink colors show the presence of Ni and Ti elements as a result of the presence of NiTi nanoparticles. As can be seen, the NiTi nanoparticles are uniformly spread with all wt.% additions.

The SEM image and EDS line scan of Ni, Mg, Zn, Ag, Ti, and O for the nanocomposites and matrix is illustrated in Fig. 7. As observed, the brighter particles of NiTi with a higher density are distributed in the matrix uniformly. Fig. 8 shows the water contact angles of the matrix and nanocomposites. Based on the measurement results, the contact angle has slightly decreased with raising the NiTi content, indicating the superior wettability for the higher content of NiTi reinforcement. The water contact angle directly reflects the surface wettability of the nanocomposites which increases the corrosion rate of the nano-composite. The increase of wettability can be due to increasing the porosity with raining the NiTi content which has been discussed in the revised manuscript.

3.3. Mechanical properties

The compressive mechanical properties of the nanocomposites as compared with the matrix, is listed in Table S1. As seen, the ultimate compressive strength and the Young's modulus of the nanocomposite have been improved with an increase in NiTi content. As compared to the matrix, the nanocomposites formability has been raised for 15 and 30 wt% NiTi content; however, it has been decreased for 45 wt% content. The strain-stress curves of nanocomposites compression test are depicted in Fig. 9a, and the UCS and elongation characteristics are illustrated in Fig. 9b graphically. 15% NiTi reinforced sample lead to an increase in compressive strength by 56% and elongation by 7.6%, as it is shown; however, further addition decreases the characteristics.

Improvements in the compressive mechanical properties can be ascribed: a) load transfer from matrix to the fairly-uniform spread NiTi particles with superior mechanical properties, b) Hall-Petch impact owing to the grain size decrease of the nanocomposites besides the NiTi content increase, c) locking dislocations owing to the hard NiTi reinforcement particle occurrence, and d) Orowan strengthening mechanism following dislocation looping formation around the NiTi particles. The potential strengthening mechanisms are illustrated in Fig. 10 schematically. Although the NiTi occurrence increased the compressive mechanical properties, the UCS and elongation were reduced with increasing NiTi in nanocomposites containing more than 15 wt% NiTi owing to the formation of brittle intermetallic phases.

The enhanced mean hardness of the nanocomposites caused by NiTi incorporation is presented in Fig. 11. The matrix with a hardness value 65.4 HV showed the raised values of 96, 122.3, and 128 HV by raising the NiTi content to 15, 30, and 45%, respectively. The values specify that 15 wt% NiTi incorporation has enhanced the matrix microhardness by 46.8%. According to the findings, the nanocomposite microhardness is higher as compared to the matrix remarkably. By a larger grain size, the Mg–3Zn-0.5Ag matrix was anticipated to hold lower mean hardness levels; however, by the smaller grain size, the composites encompassing NiTi, display higher values of hardness with the NiTi concentration increase. As harder phase (~600 Hv), the restrictions in localized deformation, triggering uniform distribution of NiTi particles, also may raise the nanocomposites hardness as compared to the matrix.

3.4. Fracture analysis

The fracture surface SEM images of the matrix and nanocomposites are demonstrated in Fig. 12. The dimples shown in Fig. 11-a1 and 11-b1 reveal that the fractures in the matrix and the nanocomposite containing lower wt.% of NiTi are ductile whereas in the case of the flat fracture surface for the nanocomposites containing higher wt.% of NiTi (Fig. 11-c1 and 11-d1), the fracture type has changed to the brittle. The images of fracture surface presented the typical shear band formations that are usually observed in the Mg-based nano-composites. The fractures are impartially brittle with little plastic deformation, as can be observed in the images. Owing to the main crack at 45° to the compression test axis,

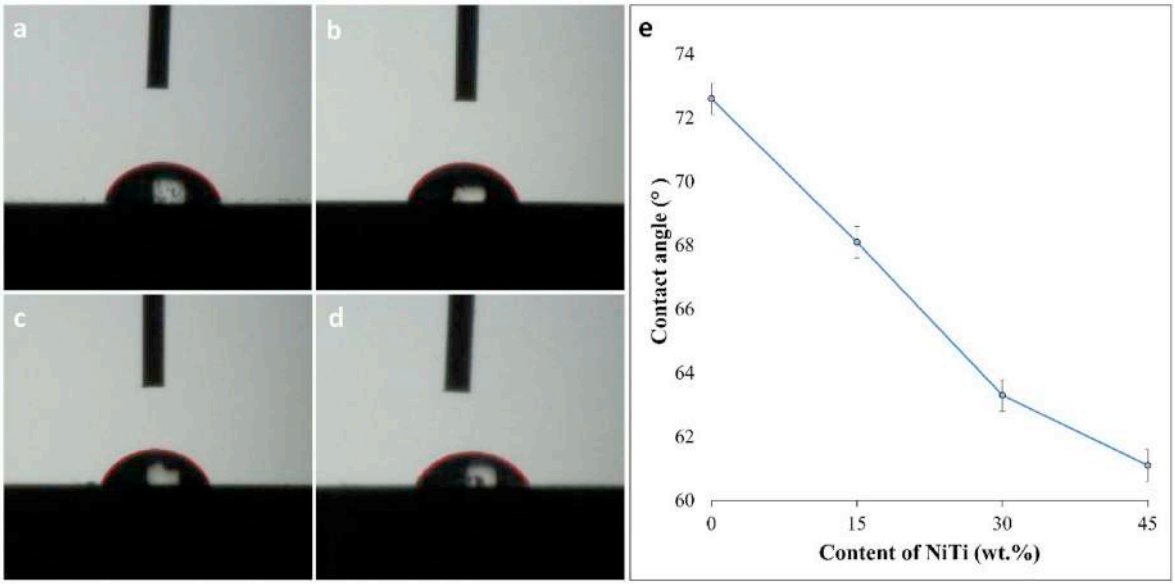

Fig. 8. Images of water contact angle of a) Matrix, b) Matrix-15NiTi, c) Matrix-30NiTi, d) Matrix-45NiTi and e) results of water contact angle test.

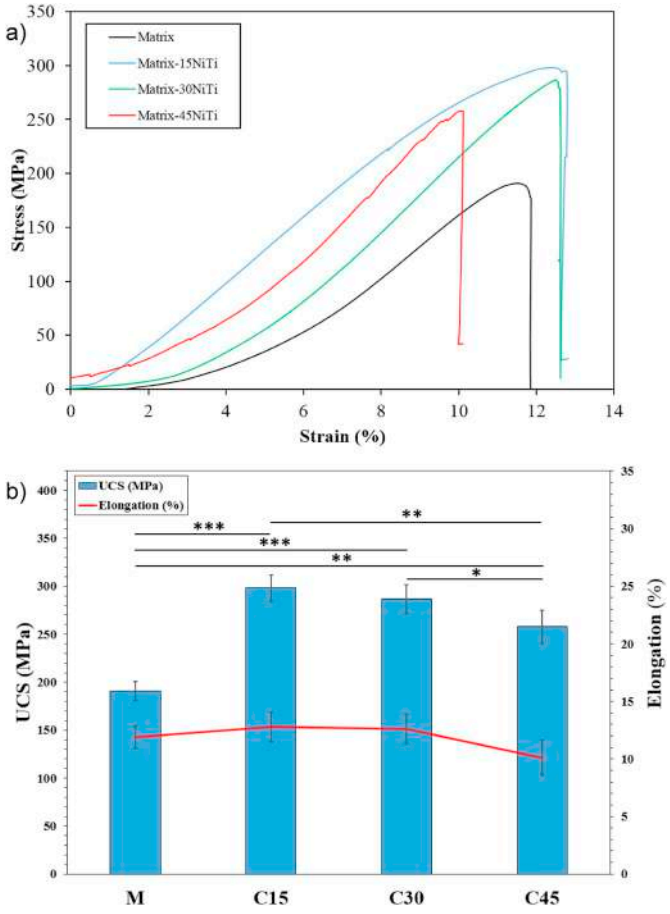

Fig. 9. a) Compressive stress-strain curve of the matrix and nanocomposites, b) Changes of UCS and elongation of M (Matrix), C15 (Matrix-15NiTi), C30 (Matrix-30NiTi) and C45 (Matrix-45NiTi) samples.

all nanocomposites were failed [50].

3.5. In-vitro biocompatibility

The short-term viability and cell attachment on the nanocomposites' surface were assessed by DAPI labeled cells; then, they were observed under the fluorescence microscope. Fig. 13A shows observations on viability live/dead staining and cell attachment that specifies certain attached cells to the substrates after incubation in the growth medium for 24 h. As can be seen, no momentous adverse effects on cell adhesion and proliferation have been perceived through 15 and 30% NiTi incorporation into the matrix; nevertheless, in the nanocomposite containing 45 wt% NiTi, both cell adhesion and proliferation are decreased. Based on the corrosion test result, for the higher content of NiTi, the degradation rate is higher. Higher degradation rate causes the production of more corrosion products which will decrease the cell adhesion of the sample. Another reason for declining cell adhesion and proliferation can be the increase of the pH value and Mg^{+2} release due to the increase in the corrosion rate of the specimen.

The nanocomposites and matrix containing NiTi have been examined for their cytotoxicity over cell proliferation test. The biomaterials cytotoxicity may be tested over MTT cell proliferation test that is assumed to decrease notably the cellular proliferation as compared to the control in the case of cytotoxic materials. The MTT test results for 24 and 48 h is specified in Table S2, and the results' graphics are displayed in Fig. 13B. According to the viability results, the nanocomposites are biocompatible on the basis of the ISO 10993-5 standard [51].

3.6. Corrosion behavior

Based on the matrix and nanocomposites potentiodynamic polarization curves (Fig. 14a), electrochemical parameters including current density and corrosion rate are derived and listed in Table S3. As it is shown, the current densities of the samples increase along with the increase of NiTi content. The corrosion rate has the same trend as the current density so that, incorporation of 15, 30 and 45 wt% of NiTi results 9.4, 50 and 287.5% increase in corrosion rate compared with the matrix.

As it can be seen, the addition of 15 wt% NiTi causes a minor increase in corrosion rate, but incorporating 30 and 45 wt% of NiTi content result a major increase in corrosion rate. Increasing the corrosion rate with

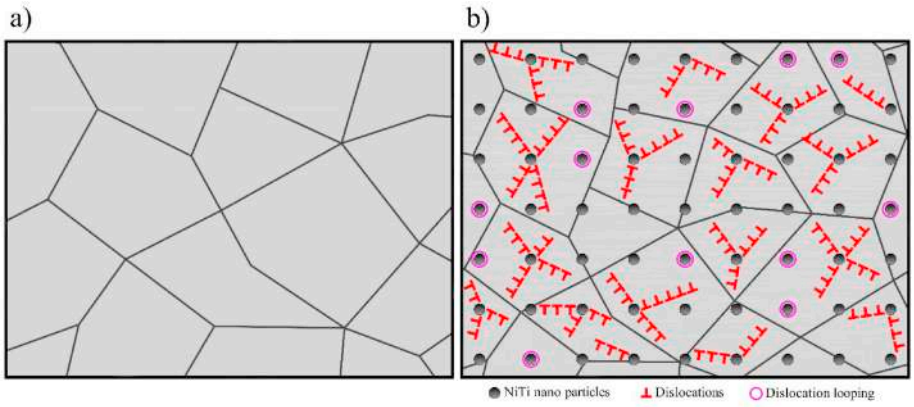

Fig. 10. Schematic illustration of the enhancement of mechanical properties due to NiTi incorporation, a) Magnesium alloy matrix b) NiTi incorporated nanocomposite.

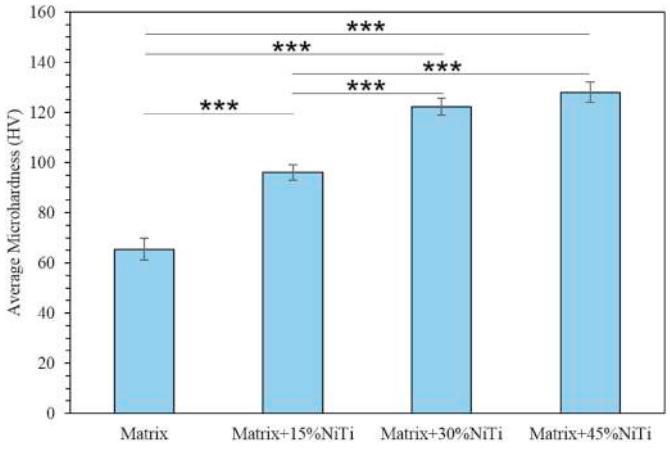

Fig. 11. Average microhardness of the nanocomposites with various NiTi content.

increment in NiTi content can be due to forming anodic locations because of the presence of NiTi particles. Small amounts of NiTi can be fairly tolerated, but the galvanic corrosion problem progressively increases for the higher contents. Higher contents of NiTi particles proceed rapidly the corrosion reactions along the interface between the Mg-based matrix and NiTi particles. The reactions lead to further penetration of electrolyte into the nanocomposite until the nanocomposite is completely destroyed [52]. Increasing the corrosion rate with augmentation in the NiTi content can be due to the formation of galvanic couples between the NiTi particles as anode and the Mg matrix as a cathode which further accelerates the corrosion process.

The described mechanism of increasing of corrosion rate of composites was also found in the study of the corrosion behavior of SiCp reinforced ZC71 metal matrix composite comparing with ZC71 magnesium alloy [53]. The average mass loss of the samples for the immersion times of 3, 7, and 14 days in Kokubo solution is shown in Fig. 14b. As can be seen, the degradation rate of the samples raised in the first period of 3 days. The reason can be the fact that the larger surface region was contacted directly by the solution in the first days of exposure, the more it causes exothermic reactions and accelerates the degradation rate. This also can be caused by the presence of a relatively high concentration of chloride in the SBF solution in the first few days [54]. With increasing the immersion time to 7 days, the degradation rate of the nanocomposite containing 15 wt% of NiTi increased with a smaller slope compared with the first 3 day of exposure. However, the nanocomposites containing 30 and 45 wt% of NiTi had lower degradation rates for this exposure time. For the immersion duration of 14 days, the degradation rates of all nanocomposites were reduced. This can be due to the reduction of the surface area of the nanocomposite that was exposed directly to the solution after the extended exposure times. In addition, the protective films from the corrosion products were formed on the surface of the nanocomposites after a longer period of immersion time. This film can reduce the degradation rate of the nanocomposites by preventing the direct exposure of nano-composites to the solution. Also, as can be observed in Fig. 14b, the addition of NiTi content from 15 to 45 wt% increased the degradation rate after 14 days. Erinc et al. proposed specific corrosion requirements of less than 0.5 mm/year for bone fixture biomaterials [55]. The test results show that the degradation rate of the nanocomposite containing 15 wt% of NiTi meets the clinical application requirement. The nanocomposite containing 15 wt% of NiTi presented lower degradation rate, implying the higher stability of the Mg composite [56–58] with lower concentration of NiTi when exposed to the SBF solution.

4. Conclusions

The mechanical alloying path followed by sintering may develop successfully magnesium-based matrix, nano-sized NiTi particles reinforced nanocomposites. In the current study, to scrutinize the practicability of Mg–3Zn–0.5Ag-xNiTi (x = 0 to 45 wt%) nanocomposites in orthopedic uses, the impacts of rising the nano-NiTi additions from 0 to 45 wt% on Mg–3Zn-0.5Ag on the nanocomposite performance measures, comprising mechanical properties and cytocompatibility were investigated. The NiTi incorporation led to decrease in the grain sizes of the Mg–3Zn-0.5Ag nanocomposite by 16.7% for the addition of 15% NiTi and raise the compressive strength by 56% and elongation by 7.6%. The nanocomposites microhardness has been raised besides increasing the NiTi incorporation in a way that NiTi 15 wt% increased the matrix microhardness by 46.8%. The addition of 15 wt% NiTi causes a minor increase in corrosion rate, but incorporating 30 and 45 wt% of NiTi content result a major increase in corrosion rate. In-vitro biocompatibility examinations have also shown that NiTi incorporation has not led to improper toxicity for the nanocomposites. The present study's general results indicate the promising applicability of bioresorbable Mg–3Zn-0.5Ag strengthened by 15 wt% NiTi nanocomposite for the implant uses.

Declaration of competing interest

The authors declare that they have no competing/financial conflict of interests in this paper.

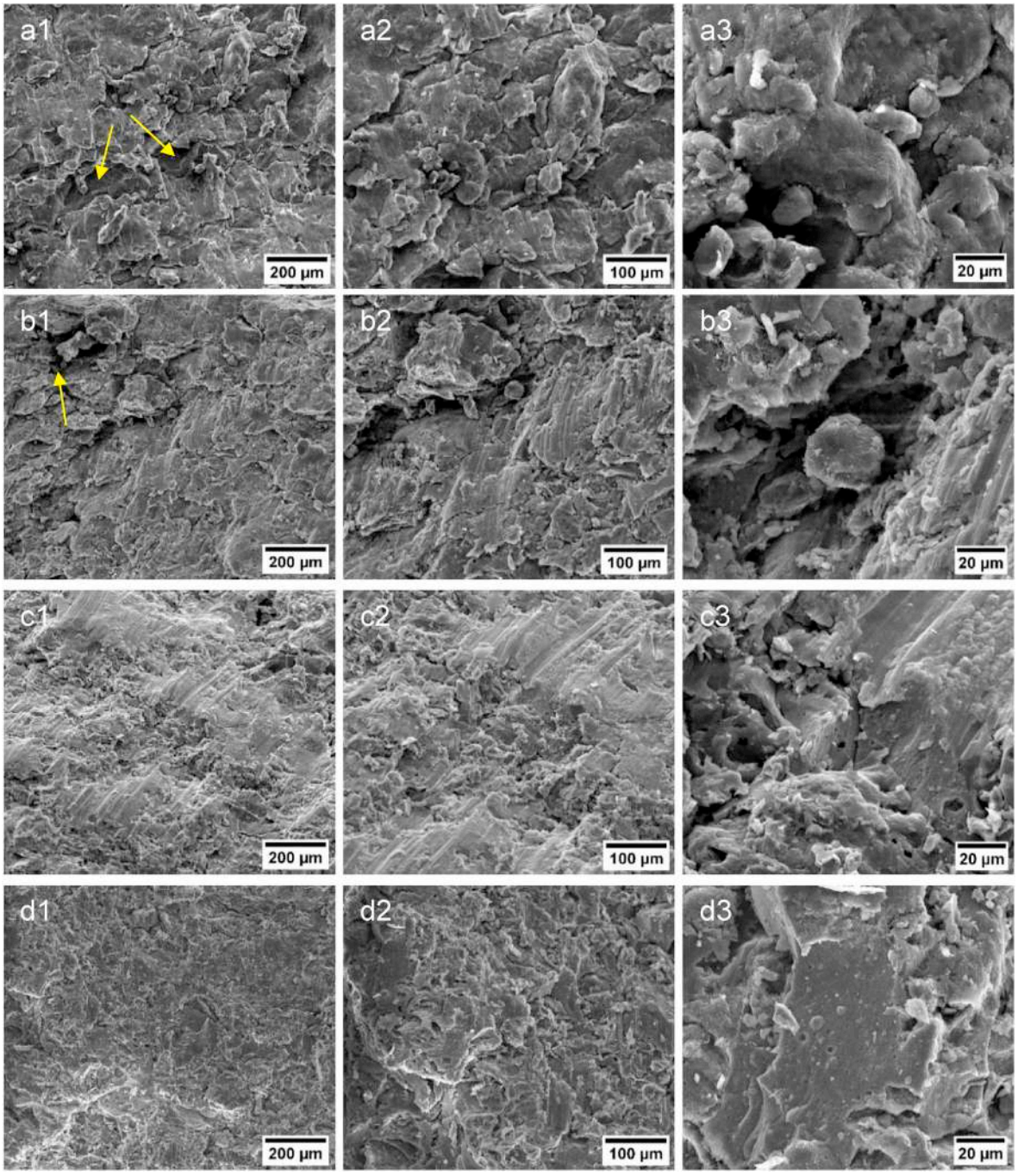

Fig. 12. SEM images of the fracture surface (a1) Matrix at ×250 magnification, (a2) Matrix at ×500 magnification, (a3) Matrix at ×2000 magnification, (b1) Matrix-15NiTi at ×250 magnification, (b2) Matrix-15NiTi at ×500 magnification, (b3) Matrix-15NiTi at ×2000 magnification, (c1) Matrix-30NiTi at ×250 magnification, (c2) Matrix-30NiTi at ×500 magnification, (c3) Matrix-30NiTi at ×2000 magnification, (d1) Matrix-45NiTi at ×250 magnification, (d2) Matrix-45NiTi at ×500 magnification, and (d3) Matrix-45NiTi at ×2000 magnification.

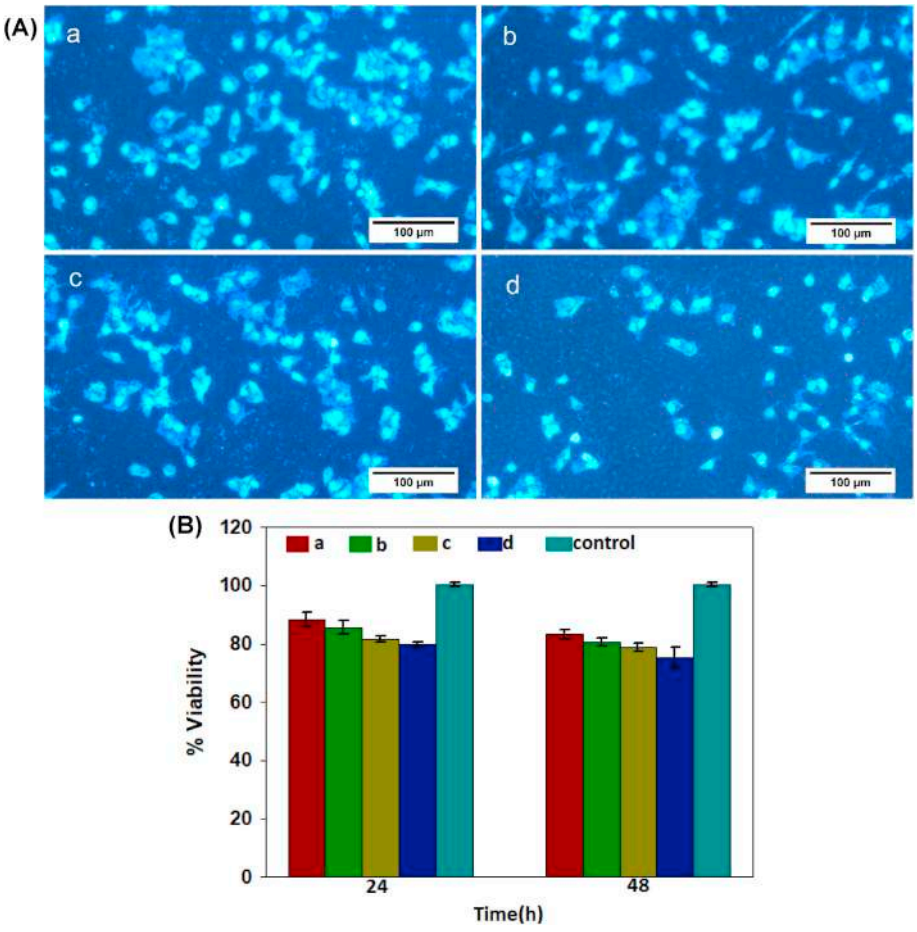

Fig. 13. (A) DAPI staining of MG63 cell cultured for 2 days, (B) Viability of MG63 osteoblast cells cultured for 24 and 48 h; For: (a) Matrix, (b) Matrix-15NiTi, (c) Matrix-30NiTi, (d) Matrix-45NiTi.

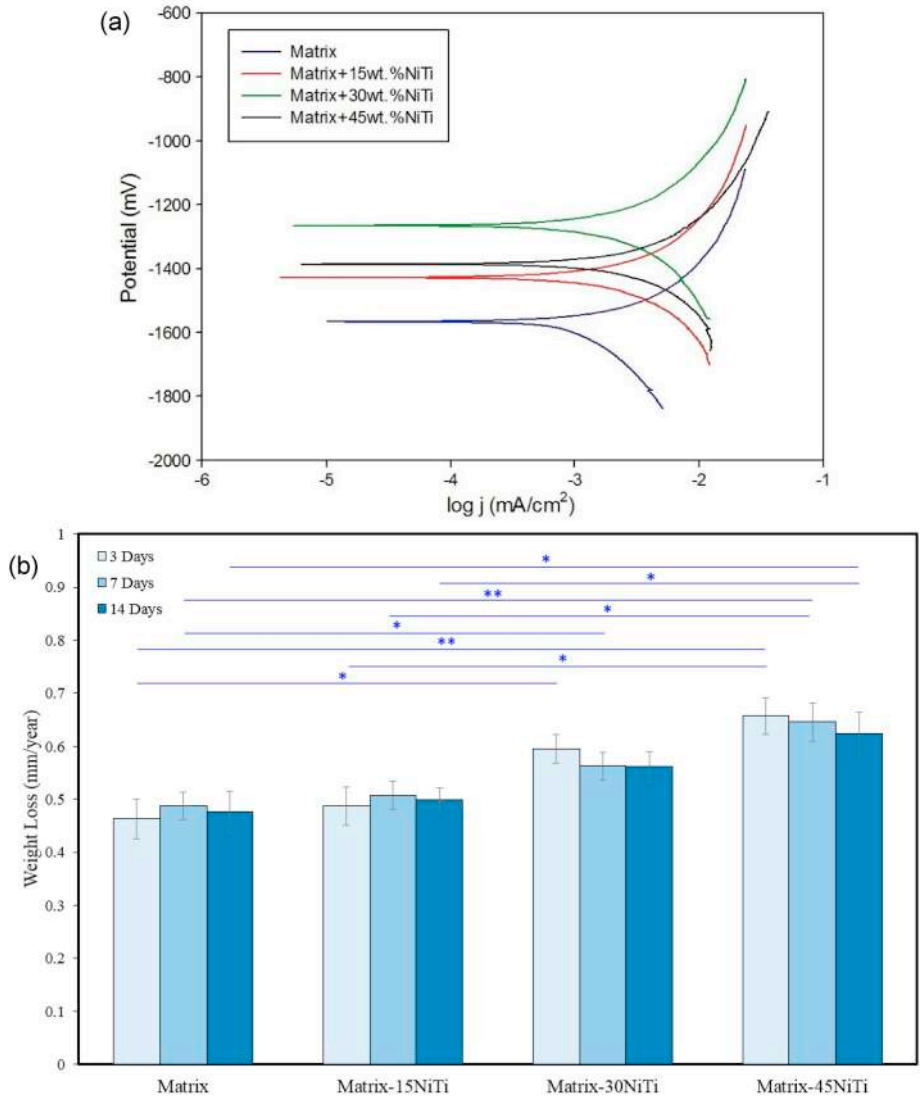

Fig. 14. (a) Potentiodynamic polarization curves of the matrix and nanocomposites with various NiTi content in SBF solution, (b) Weight loss degradation rate of the matrix and nanocomposites in Kokubo solution for the durations of 3, 7 and 14 days (*$p < 0.05$, **$p < 0.01$).

CRediT authorship contribution statement

Mahmood Razzaghi: Conceptualization, Data curation, Writing - original draft, Formal analysis. **Masoud Kasiri-Asgarani:** Supervision, Visualization, Writing - review & editing. **Hamid Reza Bakhsheshi-Rad:** Supervision, Visualization, Writing - review & editing. **Hamid Ghayour:** Supervision, Visualization, Writing - review & editing.

Acknowledgment

The authors would like to acknowledge Islamic Azad University, Najafabad for providing the research facilities.

Appendix A. Supplementary data

Supplementary data to this article can be found online at https://doi.org/10.1016/j.compositesb.2020.107947.

References

[1] Zhang LN, Hou ZT, Ye X, Xu ZB, Bai XL, Shang P. The effect of selected alloying element additions on properties of Mg-based alloy as bioimplants: a literature review. Front Mater Sci 2013;7(3):227–36.

[2] Ding P, Liu Y, He X, Liu D, Chen M. In vitro and in vivo biocompatibility of Mg–Zn–Ca alloy operative clip. Bioactive Mater 2019;4:236–44. .

[3] Waizy H, Seitz JM, Reifenrath J, Weizbauer A, Bach FW, Meyer-Lindenberg A, Denkena B, Windhagen H. Biodegradable magnesium implants for orthopedic applications. J Mater Sci 2013;48:39–50.

[4] Balakrishnan P, Sreekala MS, Thomas S, editors. Fundamental biomaterials: metals. : Woodhead Publishing; 2018.

[5] Prakasam M, Locs J, Salma-Ancane K, Loca D, Largeteau A, Berzina-Cimdina L. Biodegradable materials and metallic implants—a review. J Funct Biomater 2017;8:44.

[6] Mozafari H, Dong P, Ren K, Han X, Gu L. Micromechanical analysis of bioresorbable PLLA/Mg composites coated with MgO: effects of particle weight fraction, particle/matrix interface bonding strength and interphase, Composites Part B. 2018.

[7] Esmaily M, Mortazavi N, Svensson JE, Halvarsson M, Wessen M, Johansson LG, Jarfors AEW. A new semi-solid casting technique for fabricating SiC-reinforced Mg alloys matrix composites. Composites Part B 2016;94:176–89.

[8] Radha R, Sreekanth D. Insight of magnesium alloys and composites for orthopedic implant applications – a review. J Magnes Alloys 2017;5:286–312.

[9] Liu C, Ren Z, Xu Y, Pang S, Zhao X, Zhao Y. Biodegradable magnesium alloys developed as bone repair materials: a review. Hindawi 2018;2018:9216314.

[10] Monteiro DR, Gorup LF, Takamiya AS, Ruvollo AC, Camargo ER, Barbosa DB. The growing importance of materials that prevent microbial adhesion: antimicrobial effect of medical devices containing silver. Int J Antimicrob Agents 2009;34:103.

[11] Oluwafemi OS, Anyik JL, Zikalala NE. Biosynthesis of silver nanoparticles from water hyacinth plant leaves extract for colourimetric sensing of heavy metals. Nano-Struct Nano-Obj 2019;20:100387. .

[12] Zhu Y, Morton AJ, Nie J. Improvement in the age-hardening response of Mg–Y–Zn alloys by Ag additions. Scripta Mater 2008;58:525.

[13] Wang Q, Chen J, Zhao Z, He S. Microstructure and super high strength of cast Mg–8.5Gd–2.3Y–1.8Ag0.4Zr alloy. Mater Sci Eng, A 2010;528:323.
[14] Acikgöz S, Sevik H, Kurnaz SC. Influence of silver addition on the microstructure and mechanical properties of squeeze cast Mg–6Al–1Sn–0.3Mn–0.3Ti. J Alloys Compd 2011;509:7368.
[15] Zhang X, Zh Ba, Wang Zh, He X, Shen Ch, Wang Q. Influence of silver addition on microstructure and corrosion behavior of Mg–Nd–Zn–Zr alloys for biomedical application. Mater Lett 2013;100:188.
[16] Mandal M, Moon AP, Deo G, Mendis CL, Mondal K. Corrosion behavior of Mg–2.4Zn alloy micro-alloyed with Ag and Ca. Corrosion Sci 2014;78:172.
[17] Kavimani V, Prakash KS, Thankachan T. Experimental investigations on wear and friction behaviour of SiC@r-GO reinforced Mg matrix composites produced through solvent-based powder metallurgy. Compos B Eng 2019;162:508–21.
[18] Harrell TM, Thomsen OT, Dulieu-Barton JM, Madsen SF. Damage in CFRP composites subjected to simulated lighting strikes-Assessment of thermal and mechanical responses. Compos B Eng 2019;176:107298.
[19] Frostig Y, Thomsen OT. Non-linear thermal response of sandwich panels with a flexible core and temperature dependent mechanical properties. Compos B Eng 2008;39(1):165–84. .
[20] Charca S, Thomsen OT. Evaluation of the interface strength in metal/polymer composite systems. In: Proceeding of the 18th international conference on composite materials; 2011.
[21] Hamilton AR, Thomsen OT, Madaleno LA, Jensen LR, Rauhe JCM, Pyrz R. Evaluation of the anisotropic mechanical properties of reinforced polyurethane foams. Compos Sci Technol 2013;87:210–7. .
[22] Senis EC, Golosnoy IO, Dulieu-Barton JM, Thomsen OT. Enhancement of the electrical and thermal properties of unidirectional carbon fibre/epoxy laminates through the addition of graphene oxide. J Mater Sci 2019;54(12):8955–70. .
[23] Balakrishnan P, Sreekala MS, Geethamma VG, Kalarikkal N, Kokol V, Volova T, Thomas S. Physicochemical, mechanical, barrier and antibacterial properties of starch nanocomposites crosslinked with pre-oxidised sucrose. Ind Crop Prod 2019; 130:398–408. .
[24] Huang PS, Gao T. Current development of 1D and 2D metallic nanomaterials for the application of transparent conductors in solar cells: fabrication and modeling. Nano-Struct Nano-Obj 2018;15:119–39. .
[25] Hocheng H, editor. Machining technology for composite materials: principles and practice. : Elsevier; 2011.
[26] Augustine R, Mathew KT, Kalappura UG. Biocompatibility study of biphasic-chitosan-soya meal composite bioceramic implants and their use as phantoms for medical imaging applications. In URSI 7-16 august, 2008. 2008 [Chicago].
[27] Ninan N, Muthiah M, Park IK, Elain A, Thomas S, Grohens Y. Pectin/carboxymethyl cellulose/microfibrillated cellulose composite scaffolds for tissue engineering. Carbohydr Polym 2013;98(1):877–85. .
[28] Rouxel D, Eschbach J, Vincent B, Baret G. Brillouin scattering and tribological study of PMMA/SiO2 nanocomposite. In: New achievements in materials and environmental sciences names. : EDP Sciences; 2007. p. 79–82.
[29] Augustine R, Dan P, Sosnik A, Kalarikkal N, Tran N, Vincent B, Rouxel D. Electrospun poly (vinylidene fluoride-trifluoroethylene)/zinc oxide nanocomposite tissue engineering scaffolds with enhanced cell adhesion and blood vessel formation. Nano Res 2017;10(10):3358–76. .
[30] Tsolekile N, Parani S, Matoetoe MC, Songca SP, Oluwafemi OS. Evolution of ternary I–III–VI QDs: synthesis, characterization and application. Nano-Struct Nano-Obj 2017;12:46–56.
[31] Ghosal K, Agatemor C, Špitálsky Z, Thomas S, Kny E. Electrospinning tissue engineering and wound dressing scaffolds from polymer-titanium dioxide nanocomposites. Chem Eng J 2019;358:1262–78. .
[32] Esen Z. TiNi reinforced magnesium composites by powder metallurgy. TMS miner, Metals Mater Soc) 2011;30:457–62.
[33] Es-Souni M, Es-Souni M, Fischer-Brandies H. Assessing the biocompatibility of NiTi shape memory alloys used for medical applications. Anal Bioanal Chem 2005;381 (3):557–67.
[34] Bansiddhi A, Sargeant TD, Stupp SI, Dunand DC. Porous NiTi for bone implants: a review. Acta Biomater 2008;4(4):773–82. .
[35] Guo W, Kato H, Lü S, Wu S. Porous NiTi particle dispersed Mg-Zn-Ca bulk metallic glass matrix composites. Materials 2018;11:1959.
[36] Esen Z. The effect of processing routes on the structure and properties of magnesium-TiNi composites. Mater Sci Eng 2012;558:632–40.
[37] Wakeel S, Manakari V, Parande G, Suchita Kujur M, Ahmad khana A, Gupta M. Synthesis and mechanical response of NiTi SMA nanoparticle reinforced Mg composites synthesized through microwave sintering process. Mater Today: Proc 2018;5:28203–10.
[38] Khalajabadi SZ, Kadir MRA, Izman S, Bakhsheshi-Rad HR, Farahany S. Effect of mechanical alloying on the phase evolution, microstructure and bio-corrosion properties of a Mg/HA/TiO_2/MgO nanocomposite. Ceram Int 2014;40:16743.
[39] Sharma S, Susan D, Kothiyal NC, Kaur R. Graphene oxide prepared from mechanically milled graphite: effect on strength of novel fly-ash based cementitious matrix. Construct Build Mater 2018;177:10–22.
[40] Pereda MD, Alonso C, Burgos-Asperilla L, del Valle JA, Ruano OA, Perez P, Fernández Lorenzo de Mele MA. Corrosion inhibition of powder metallurgy Mg by fluoride treatments. Acta Biomater 2010;6:1772.
[41] Datta MK, Chou DT, Hong D, Saha P, Chung SJ, Lee B, Sirinterlikci A, Ramanathan M, Roy A, Kumta PN. Structure and thermal stability of biodegradable Mg–Zn–Ca based amorphous alloys synthesized by mechanical alloying. Mater Sci Eng B 2011;176:1637.
[42] Liang G, Schulz R. Synthesis of binary Mg-based alloys by mechanical alloying. J Metastable Nanocryst Mater 2002;12:93–110.
[43] Salleh EM, Ramakrishnan S, Hussain Z. Synthesis of biodegradable Mg-Zn alloy by mechanical alloying: effect of milling time. Procedia Chem 2016;19:525–30.
[44] Askeland DR, Fulay PP, Wright WJ. The science and engineering of materials. 6 ed. Cengage Learning Inc.; 2011.
[45] Williamson GK, Hall WH. X-ray line broadening from filed aluminum and wolfram. Acta Metall 1953;1:22.
[46] Zheng YF, Gu XN, Xi YL, Chai DL. In vitro degradation and cytotoxicity of Mg/Ca composites produced by powder metallurgy. Acta Biomater 2010;6:1783.
[47] ASTM. Standard practice for preparing, cleaning, and evaluating corrosion test specimens (G1-03). 2011.
[48] Seif Fathy A, Wagih A, Abd El-Hamid M, Hassan AA. Effect of mechanical milling on the morphology and structural evaluation of Al-Al_2O_3 nanocomposite powders. IJE Trans A: Basics April 2014;27(No. 4):625–32.
[49] Khalifa ZS. Grain size reduction on nanostructured TiO 2 thin films due to annealing. RSC Adv 2017;7(48):30295–302.
[50] [81] Suneesh E, Sivapragash M. Compressive and impact responses OF magnesium/alumina composites. Technology 2017;8(8):472–8.
[51] International Organization for Standardization. Biological evaluation of medical devices- Part 5: tests for in-vitro cytotoxicity (ISO10993-5). 2009.
[52] Ferrando WA. Review of corrosion and corrosion control of magnesium alloys and composites. J Mater Eng 1989;11:299–313.
[53] Nunez-Lopez CA, Skeldon P, Thompson GE, Lyon P, Karimzadeh H, Wilks TE. Corrosion Sci 1995;37:689.
[54] Bakhsheshi-Rad HR, Idris MH, Abdul-Kadir MR, et al. Mechanical and bio-corrosion properties of quaternary Mg–Ca–Mn–Zn alloys compared with binary Mg–Ca alloys. Mater Des 2014;53:283.
[55] Erinc M, Sillekens WH, Mannens R, Werkhoven RJ. Applicability of existing magnesium alloys as biomedical implant materials. In: Nyberg EA, Agnew SR, Neelameggham NR, Pekguleryuz MQ, editors. Magnesium technology; 2009. p. 209–14. San Francisco.
[56] Bakhsheshi-Rad HR, Hamzah E, Ismail AF, Kasiri-Asgarani M, et al. Novel bi-layered nanostructured SiO_2/Ag-FHAp coating on biodegradable magnesium alloy for biomedical applications. Ceram Int 2016;42:11941–50.
[57] Bakhsheshi-Rad HR, Hamzah E, Kasiri-Asgarani M, et al. Fabrication, degradation behavior and cytotoxicity of nanostructured hardystonite and titania/hardystonite coatings on Mg alloys. Vacuum 2016;129:9–12.
[58] Saheban M, Bakhsheshi-Rad HR, Kasiri-Asgarani M, et al. Effect of zeolite on the corrosion behavior, biocompatibility and antibacterial activity of porous magnesium/zeolite composite scaffolds. Mater Technol 2019;34:258–69.